BB

SAGA-HE-69-94
September 1994

Optical potential near Fermi surface by nuclear Schwinger-Dyson equations with bare vertex approximation

Akira HASEGAWA, Tomohiro MITSUMORI, Masaru MURAKI
Kazuharu KOIDE and Hiroaki KOUNO
Department of Physics, Saga University, Saga 840, Japan
and
Masahiro NAKANO
University of Occupational and Enviromental Health
Kitakyushu 807, Japan

Optical potential near Fermi surface are calculated under the bare vertex nuclear Schwinger-Dyson method based on the $\sigma - \omega$ model, making use of results on nuclear matter. Saturation and liquid-vapor instability of nuclear matter are discussed. Contributions of mesons affected by nuclear medium in the optical potential are clarified. The ω-meson contribution is prominently large and originates in the difference between the transverse and the longitudinal components of ω-meson propagator, and this difference vanishes without nuclear medium. As a result the effective mass of nucleon increases rapidly near the Fermi energy and the ω-meson dominance near the Fermi surface in the imaginary potential agrees with the result in the non-relativistic Hartree-Fock calculation.

1. Introduction

The nuclear matter is an useful subject to study strongly interacting many-body system in the quantum hadrodymamics. In the last five years, two loop and ring-correlation corrections have been calculated in terms of the renormalizable $\sigma - \omega$ model. Computational results[1)~4)] showed that the one loop diagram was not the leading term in the loop expansion since these two corrections contributed much to the energy density, both in a vacuum fluctuation part and in a finite density part, respectively. Furthermore, the vacuum polarization in ω-meson propagator generated ghost poles in the high momentum transfer region($>$ a few GeV) and this instability was present at all densities. This means that the mean field is inevitably unstable[4)].

The enormously large loop corrections in a vacuum part were reduced to moderate ones by introducing form factors at all vertices in the loop diagram[5),6)], and the ghost poles were removed by vertex corrections to vacuum polarization[7)]. Though the inserted form factors were ad hoc ones and vertex corrections were restricted to the on-shell vertex, these procedures for reducing short-distance contributions are qualitatively acceptable at present to consider the subnucleon structure. Anyway, it is an important prospect that contributions from vacuum polarization loops and from vertex modifications will cancel out each other in the high momentum transfer region.

To a density part of nuclear matter, as well as to finite nuclei[8)], we applied the Schwinger-Dyson equations with bare vertex approximation(the BNSD method)[9)] and showd that medium effects on meson played an important role in the saturation property of nuclear matter[10),11)]. In the BNSD approximation we do not consider vacuum corrections from the above discussed prospect. Large meson self-energies in meson propagators brought about attractive contributions in the SD terms, an abbreviation for the quantum corrections fluctuating around the mean field, in energy density and self-energy of nucleon. On the other hand, the strong $\sigma - \omega$ mixing through the polarization process gave repulsive contributions to the SD terms. The saturation property was explained by the drastic cancelation between the σ-meson and the ω -meson contributions both in the classical mean field and in the SD quantum field. In the quantum field the $\sigma - \omega$ mixing made this cancellation more drastic, and the quantum corrections were small in comparison with the mean field contribution. In the saturated state of nuclear matter, medium effects on meson made coupling parameters small and as a result an unstable region, which appeared at low density and has been interpreted as a liquid-vapor phase transition, was shifted above the normal density. There were shown some recipes to remove this instability.

In this paper we evaluate an optical potential for nucleon traveling in the neighborhood of the Fermi surface, according to the BNSD method and making use of results of nuclear matter. This is the first step to apply the Schwinger-Dyson equation to scattering problem. In particular, we note an imaginary potential since this potential is drawn out only from the SD quantum term of nucleon self-energy. Then, the imaginary potential is sensitive to the SD terms. We clarify contributions of each meson and the mixing of meson both in the real potential and in the imaginary potential. To make sure that the BNSD method is valid even in phenomena explained well by non-relativistic calculations[12)], we compare our results with the same empirical information[18),19)].

The outline of the paper is as follows. In sect.2, we derive optical potential and explain our approximations adopted there. In sect.3 we show a calculation on nuclear matter removing the instability under a new recipe. In sect.4, we show calculation results and discussions, and sect.5 is devoted to remarks and summary.

2. Derivation of optical potential

We adopt the Walecka model[13)] which consists of three fields, the nucleon ψ, the scalar σ-meson ϕ and the vector ω -meson V_ν. The lagrangian density is given by

$$L = -\bar{\psi}(\gamma_\mu \partial_\mu + M)\psi - \frac{1}{2}(\partial_\mu \phi \partial_\mu \phi + m_s^2 \phi^2)$$

$$-(\frac{1}{4}F_{\mu\nu}F_{\mu\nu} + \frac{1}{2}m_v^2 V_\mu V_\mu) + g_s \bar{\psi}\psi\phi + i g_v \bar{\psi}\gamma_\mu \psi V_\mu, \qquad (1)$$

where $F_{\mu\nu} = \partial_\mu V_\nu - \partial_\nu V_\mu$ and M, m_s, m_v, g_s and g_v are nucleon mass, σ-meson mass, ω-meson mass, σ-nucleon and ω-nucleon coupling-constants respectively.

The nuclear Schwinger-Dyson equations are shown diagrammatically in Fig.1. The doubly wavy lines show propagators of mesons carrying a non- vanishing momentum, while mesons with zero four-momentum are condensed into the ground state and contribute to mean field energies of the ground state, and appear as the Hartree fields in the Dyson equation of nucleon propagator. In the BNSD approximation vertex functions are same with the bare vertex in the lagrangian Eq.(1), i.e., $\Gamma_a = 1$ for σ-meson and $\Gamma_a = \gamma_\mu$ for ω-meson.

Fig.1

The nucleon propagator $G(k)$ has a standard form

$$G(k) = G_F(k) + G_D(k)$$

$$= \frac{-1}{i\gamma_\mu k^*_\mu + M^*_k - i\epsilon} + (-i\gamma_\mu k^*_\mu + M^*_k)\frac{i\pi}{E^*_k}\delta(k^*_0 - E^*_k)\theta(k_F - |\mathbf{k}|), \tag{2}$$

$$E^*_k = \sqrt{k^{*2} + M^*_k}, \tag{3}$$

$$M^*_k = M + \Sigma_s(k), \tag{4}$$

$$k^*_\mu = \Big(\mathbf{k}(1 + \Sigma_v(k)), k_4 + \Sigma_4(k))\Big) = \Big(\mathbf{k}(1 + \Sigma_v(k)), i(k_0 + \Sigma_0(k))\Big), \tag{5}$$

where the self-energy insertion is assumed as follows

$$\Sigma(k) = \Sigma_s(k) + i\gamma_4\Sigma_4(k) + i\gamma_i \cdot k_i\Sigma_v(k)$$

$$= \Sigma_s(k) - \gamma_0\Sigma_0(k) + i\gamma_i \cdot k_i\Sigma_v(k). \tag{6}$$

To explain derivation of imaginary part of self-energy under our approximations, we consider only the σ-meson in the following discussion. The σ-meson propagator is given by SD equation

$$D(q) = ReD(q) + iImD(q)$$

$$= -\frac{q^2 + m_s^2 + Re\Pi_s(q)}{(q^2 + M_s^2 + Re\Pi_s(q))^2 + (Im\Pi_s(q))^2} + i\frac{Im\Pi_s(q)}{(q^2 + M_s^2 + Re\Pi_s(q))^2 + (Im\Pi_s(q))^2} \tag{7}$$

where $\Pi_s(q)$ denotes the meson self-energy. The self-energy of nucleon propagating nearly above the Fermi surface consists of three terms, the Hartree term Σ_H, the SD density term Σ_{SDD} and the SD Feynman term Σ_{SDF},

$$\Sigma(k) = \Sigma_H(k) + \Sigma_{SDF}(k) + \Sigma_{SDD}(k)$$

$$= i\tau\left(\frac{g_s}{m_s}\right)^2 \int \frac{d^4q}{(2\pi)^4} tr\Big(G(q)\Big) + ig_s^2 \int \frac{d^4q}{(2\pi)^4} G_F(k-q)D(q)$$

$$+ig_s^2 \int \frac{d^4q}{(2\pi)^4} G_D(k-q)D(q), \tag{8}$$

where τ denotes the degeneracy, τ=2 for nuclear matter and τ=1 for neutron matter. The Hartree term $\Sigma_H(k)$ is real and is evaluated by using only the density part of propagator $G_D(k-q)$ in the BNSD approximation. The SD density term $\Sigma_{SDD}(k)$ is finite and has a real part and a imaginary part corresponding with the real part and the imaginary part of meson propagator $D(q)$ respectively. The SD Feynman term $\Sigma_{SDF}(k)$ has a infinite real part and a finite imaginary part. To separate the real part and the imaginary part, we execute a Wick rotation $q_0 \rightarrow iq_0$ in the q_0 integral in $\Sigma_{SDF}(k)$

$$\Sigma_{SDF}(k) = g_s^2 \int \frac{d^3q}{(2\pi)^3}\frac{i}{2\pi}\int_{-i\infty}^{i\infty} dq_0 G_F(k-q)D(q)$$

$$-ig_s^2 \int \frac{d^4q}{(2\pi)^4}(-i\gamma_\mu(k-q)^*_\mu + M^*_{k-q})\frac{\pi i}{E^*_{k-q}}\delta((k-q)^*_0 - E^*_{k-q})\theta(k_0 - E_{k-q})ReD(q)$$

$$-ig_s^2\int\frac{d^4q}{(2\pi)^4}(-i\gamma_\mu(k-q)^*_\mu+M^*_{k-q})\frac{\pi i}{E^*_{k-q}}\delta((k-q)^*_0-E^*_{k-q})\theta(k_0-E_{k-q})iImD(q) \quad (9)$$

The first term is real and infinite. The second term is also real but finite. We, however, do not pick up this term since these two real terms are derived by considering the Feynman part of propagator $G_F(k-q)$ and the real part of $\Sigma_{SDF}(k)$ should be originally infinite without a procedure of renomalization. The third term is purely imaginary and finite. Adding contribitions from $\Sigma_H(k)$ and $\Sigma_{SDD}(k)$, the real and the imaginary parts of self-energy are given by

$$Re\Sigma(k)=i\tau\frac{g_s^2}{m_s^2}\int\frac{d^4q}{(2\pi)^4}tr(G_D(q))$$

$$+ig_s^2\int\frac{d^4q}{(2\pi)^4}(-i\gamma_\mu(k-q)^*_\mu+M^*_{k-q})\frac{\pi i}{E^*_{k-q}}\delta((k-q)^*_0-E^*_{k-q})\theta(k_F-|\mathbf{k}-\mathbf{q}|)ReD(q) \quad (10)$$

$$Im\Sigma(k)=ig_s^2\int\frac{d^4q}{(2\pi)^4}(-i\gamma_\mu(k-q)^*_\mu+M^*_{k-q})\frac{\pi i}{E^*_{k-q}}\delta((k-q)^*_0-E^*_{k-q})$$

$$\times[-\theta(k_0-E_{k-q})+\theta(k_F-|\mathbf{k}-\mathbf{q}|)]iImD(q) \quad (11)$$

In Fig.2 we show Feynman diagrams taken into account in our calculation of nucleon self-energy $\Sigma(k)$.

Fig.2

For calculations of real self-energy we take a hole state on shell as an intermediate state of nucleon. On the other hand, in the derivation of imaginary part of self-energy a particle state on shell is needed as an intermediate state . This is a reasonable result because the imaginary self- energy in a scattering state means a real 2p-1h process that the nucleon traveling above the Fermi surface loses its energy partialy to cause a particle-hole excitation through the decay of meson.

We also derive ω-meson contribution in the imaginary self-energy in the same procedure explained above. By taking an important role of the $\sigma-\omega$ mixing into account[14], we use a 5x5 unified expression $D_{ab}(q)$ for the σ- and the ω-meson propagators and we provide a general expression for meson self-energy $\Pi_{ab}(q)$ to calculate the nucleon self-energy. The insertion $\Pi_{ab}(q)$ and the meson propagator $D_{ab}(q)$ in the general expression are given in Ref.10).

Under the same approximations with those assumed in derivation of Eqs.(10) and (11), the self-energy of a nucleon propagating above the Fermi surface are given by

$$Re\Sigma_s(k)=-\frac{\tau}{\pi^2}\frac{g_s^2}{m_s^2}\rho_s+\frac{g_s^2}{8\pi^2}\int_0^{k_F}q^2\frac{M^*_q}{E^*_q}dq\int_{-1}^{1}dxReD_s(R)$$

$$-\frac{g_v^2}{8\pi^2}\int_0^{k_F}q^2\frac{M^*_q}{E^*_q}dq\int_{-1}^{1}dx\{4ReD_l(R)+(3+\frac{R_0^2}{\vec{R}^2})(ReD_t(R)-ReD_l(R))\}$$

$$+\frac{g_sg_v}{4\pi^2}\int_0^{k_F}q^2dq\int_{-1}^{1}dxReD_m(R)\frac{R^2}{\vec{R}^2}, \quad (13a)$$

$$Im\Sigma_s(k)=\frac{g_s^2}{8\pi^2}\int_{k_F}^{k}q^2\frac{M^*_q}{E^*_q}dq\int_{-1}^{1}dxImD_s(R)$$

$$-\frac{g_v^2}{8\pi^2}\int_{k_F}^{k}q^2\frac{M^*_q}{E^*_q}dq\int_{-1}^{1}dx\{4ImD_l(R)+(3+\frac{R_0^2}{\vec{R}^2})(ImD_t(R)-ImD_l(R))\}$$

$$+\frac{g_sg_v}{4\pi^2}\int_{k_F}^{k}q^2dq\int_{-1}^{1}dxImD_m(R)\frac{R^2}{\vec{R}^2}, \quad (13b)$$

$$Re\Sigma_0(k) = -\frac{\tau}{\pi^2}\frac{g_v^2}{m_v^2}\frac{k_F^3}{3} - \frac{g_s^2}{8\pi^2}\int_0^{k_F} q^2dq \int_{-1}^{1} dx ReD_s(R)$$

$$+\frac{g_v^2}{8\pi^2}\int_0^{k_F} q^2dq \int_{-1}^{1} dx\{2ReD_l(R) + (2+\frac{R^2}{\vec{R}^2})(ReD_t(R) - ReD_l(R))\}$$

$$+\frac{g_s g_v}{4\pi^2}\int_0^{k_F} q^2dq \int_{-1}^{1} dx \frac{M_q^*}{E_q^*} ReD_m(R)\frac{R^2}{\vec{R}^2}, \qquad (14a)$$

$$Im\Sigma_0(k) = -\frac{g_s^2}{8\pi^2}\int_{k_F}^{k} q^2dq \int_{-1}^{1} dx ImD_s(R)$$

$$-\frac{g_v^2}{8\pi^2}\int_{k_F}^{k} q^2dq \int_{-1}^{1} dx\{2ImD_l(R) + (2+\frac{R^2}{\vec{R}^2})(ImD_t(R) - ImD_l(R))\}$$

$$-\frac{g_s g_v}{4\pi^2}\int_{k_F}^{k} q^2dq \int_{-1}^{1} dx \frac{M_q^*}{E_q^*} ImD_m(R)\frac{R^2}{\vec{R}^2}, \qquad (14b)$$

$$Re\Sigma_v(k) = -\frac{g_s^2}{8\pi^2 k}\int_0^{k_F} \frac{q^2q^*}{E_q^*}dq \int_{-1}^{1} dx\, x ReD_s(R)$$

$$-\frac{g_v^2}{8\pi^2 k^2}\int_0^{k_F} q^2dq \int_{-1}^{1} dx \frac{q^*kx}{E_q^*}\{2ReD_l(R) + (2-\frac{R^2}{\vec{R}^2})(ReD_t(R) - ReD_l(R))\}, \qquad (15a)$$

$$Im\Sigma_v(k) = -\frac{g_s^2}{8\pi^2 k}\int_{k_F}^{k} \frac{q^2q^*}{E_q^*}dq \int_{-1}^{1} dx\ \ xImD_s(R)$$

$$-\frac{g_v^2}{8\pi^2 k^2}\int_{k_F}^{k} q^2dq \int_{-1}^{1} dx \frac{q^*kx}{E_q^*}\{2ImD_l(R) + (2-\frac{R^2}{\vec{R}^2})(ImD_t(R) - ImD_l(R))\}, \qquad (15b)$$

where $R = k - q$, and ρ_s and ρ_B denote the scalar and the baryon densities respectively. We can have $Im\Sigma(k)$ of a hole under the Fermi surface when the upper limit k is smaller then the Fermi momentum k_F in Eqs.(13)$\sim$(15). We note that we obtain the lowest order contribution [12),15),16)] in the imaginary part of nucleon self-energy when we rewrite imaginary parts of meson propagators in Eqs.(13b),(14b) and (15b) as follows

$$ImD_s = (D_s^0)^2 Im\Pi_s \ \ , \ \ ImD_l = (D_v^0)^2 Im\Pi_l,$$

$$ImD_t = (D_v^0)^2 Im\Pi_t \ \ , \ \ ImD_m = -D_s^0 D_v^0 Im\Pi_m, \qquad (16)$$

where $D_s^0(q)$ and $D_v^0(q)$ denote the non-interacting propagators of σ- and ω-mesons respectively. The subscripts s, l, t and m of $D(q)$ and $\Pi(q)$ in Eq.(13a)$\sim$Eq.(16) denote the component of σ-meson, the longitudinal and the transverse components of ω-meson and the component of mixture of σ- and ω-mesons respectively.

Optical potentials in the relativistic form are defined from self- energies Σ as

$$U_S = \frac{(\Sigma_s - M\Sigma_v)}{(1+\Sigma_v)} = U_{SR} + iU_{SI}, \qquad (17)$$

$$U_V = \frac{(-\Sigma_0 + E\Sigma_v)}{(1+\Sigma_v)} = U_{VR} + iU_{VI}, \qquad (18)$$

where E is the energy of objective nucleon propagating through nuclear matter and relates with the momentum k in the following dispersion relation

$$E = \sqrt{\mathbf{k}^2 + (M + U_S)^2} + U_V, \tag{19}$$

This equation is rewitten as

$$\frac{\mathbf{k}^2}{2M} + V + iW = E - M + \frac{(E-M)^2}{2M}, \tag{20}$$

with Schrödinger equivalent potential form

$$V = U_{SR} + U_{VR} + \frac{(E-M)^2}{M} U_{VR} + \frac{1}{2M}(U_{SR}^2 + U_{VI}^2 - U_{SI}^2 - U_{VR}^2), \tag{21}$$

$$W = U_{SI} + U_{VI} + \frac{(E-M)^2}{M} U_{VI} + \frac{1}{M}(U_{SR}U_{SI} - U_{VR}U_{VI}). \tag{22}$$

3. Saturation and instability of nuclear matter

In calculations of nucleon and meson self-energies we use coupling parameters, g_s and g_v, obtained in the study of nuclear matter on basis of the BNSD approximation. These parameters are determined to get the minimum energy at the normal density and simultaneously to remove an instability which comes from σ-meson poles caused by nuclear medium. There have been shown some recipes to remove this instability. Bedau and Beck[1] removed this by inserting an ad hoc Migdal parameter into the σ-meson self-energy. We also made efforts for the removal of instability. The first attempt[10] was very easy, i.e., to add a small positive constant in the denominator of σ-meson propagator. We expected that the meson self-energy was calculated under many approximations and so the instability might diminish spontaneously by using the exact self-energy. The second attempt[11] was to change the σ-meson mass as a parameter as well as coupling parameters to get the saturation energy. The small σ-meson mass obtained there, 300 MeV $\sim$ 350 MeV, seemed to be the result affected by neglecting vacuum effects and vertex corrections.

In this paper we consider effects of vacuum polarization in meson self-energy[4] to remove the instability. This seems to be inconsistent with the BNSD approximation. However, as long as we choice only a hole state as an intermediate state in the integral in the nucleon self-energy $\Sigma(k)$, the vacuum polarization is restricted to the one with low four-momentum transfer. Vertex modifications or form factors are needed to reduce the vacuum polarization with large four-momentum transfer. In Fig.3 we show an example of the meson self-energy $\Pi(q)$ as a function of transferd energy q_0 by fixing a transferd momentum q=100 MeV. In this example the $\Pi(q)$ for $q_0 < 25$ MeV is available in the calculation of $\Sigma(k)$ under our approximation and in this available region effects of vacuum polarization are very small except for the effect in σ-meson self-energy, which gives a nearly constant increase. As shown in Fig.3(b), effects of all vacuum polarizations in the available region are extremely small compared with ones in the GeV region.

Fig.3

Instability modes at zero energy transfer are obtained from the zeros of the longitudinal dielectric function, i.e.,

$$\epsilon_L(q_0 = 0, q) = (q^2 + M_s^2 + \Pi_s(q))(q^2 + M_v^2 + \Pi_l(q)) + \{\Pi_m(q)\}^2 \tag{23}$$

We have never instability modes when the above dielectric function is positive for all momenta q. The vacuum polarization of σ-meson play an important role to have the dielectric function keep positive by reducing the σ-meson self-energy.

The saturation property of binding energy and the dielectric function are shown in Fig.4 and in Fig.5, respectively.In Fig.5,for reference,we add a result excluding the vacuum polarization of meson.

Fig.4 , Fig.5

Obtained coupling parameters are summarized in Table together with ones[17] obtained by the Hartree-Fock approximation. The energy density per nucleon is divided into the nucleon energy ϵ_B, the condensed energy ϵ_C and the SD energy ϵ_{SD}, and they are also shown in Table. We note that the coupling parameters obtained in the two methods are very similar. However,the ratio of the SD contribution to binding energy is about 5% of the Hartree contribution and firms our conclusion in the previous paper[11]. Also, the nearly constant and positive vacuum correction corresponds effectively with the small σ-meson mass and the small coupling-constant obtained without vacuum polarization on meson in Ref.11), and however we can not compare them quantatively since the coupling parameters searched in each model are very different.

Table

4. Calculation results and discussions

In this section we calculate the self-energy of nucleon propagating nealy above the Fermi surface with its energy E and obtain the optical potential in the Schrödinger equivalent form. We note some comments on procedure of calculation before we show results and discuss them. The momentum k of nucleon with the energy E is determined by the following relation

$$E = \sqrt{k^2(1 + Re\Sigma_v(E,k))^2 + (M + Re\Sigma_s(E,k))^2} - Re\Sigma_0(E,k), \qquad (24)$$

which is the same as the real part of Eq.(19).Only in calculations of meson self-energies we adopt the averaged self-energy of nucleon. This means that we need calculate all $Re\Sigma(E',k')$ for $E_F < E' < E$ and $k_F < k' < k$. After all we have to solve iteratively the dispersion relation similar to Eq.(24) from the Fermi momentum to the momentum of the objective nucleon.

We start with the real part of meson self-energy. The real part $Re\Sigma$ as a function of $E-M$ is shown in Fig.6 in comparison with the one by the Hartree-Fock(HF) calculation. The energy dependence of $Re\Sigma$ is produced by the SD term in the BNSD method and by the Fock term in the HF method respectively since the Hartree term has not an energy-dependence both in two methods. Though the Schrödinger equivalence potential is almost same in the two methods because it is given roughly by a difference $Re\Sigma_s - Re\Sigma_0$ as shown in Eq.(21), the effective mass of nucleon, $M + Re\Sigma_s$, in the BNSD method shows a rapid increase in the energy region $E_F - M < E - M < -E_F + M$, while the nucleon mass in the HF method shows a slowly varying energy- dependence.

Fig.6

In Fig.7, to analyse the energy-dependence we show contributions of σ-meson, ω-meson and $\sigma - \omega$ mixture in the SD terms in $Re\Sigma_s$ and in $Re\Sigma_0$ respectively. Values of $Re\Sigma_v$ are negligiblely small in comparison with 1 and are not shown in this figure. Signs of contributions of each meson and $\sigma - \omega$ mixture are easy undrstood with reference to the expressions of SD terms in Eqs.(13a), (14a) and (15a) and to the energy-dependence of propagators, $D_s(R), D_l(R), D_t(R)$ and $D_m(R)$ shown in Fig.8. The contributions of σ-meson and $\sigma - \omega$ mixture cancel each other both in $Re\Sigma_s$ and in $Re\Sigma_0$, and so the

ω-meson contribution is very important in the energy-dependence of $Re\Sigma$. We note that the term with a difference $ReD_t(R) - ReD_l(R)$ in the integral in $Re\Sigma$ is the main part of ω-meson contribution. This difference of the transverse and the longitudinal components of ω-meson propagator never appears in the Fock term in the HF method since the two components of free ω-meson propagator are same, $D_t^0(R) = D_l^0(R)$.

Fig.7 , Fig.8

Next, we discuss the imaginary part of self-energy. We note that this imaginary part is drawn out only from the SD term in the BNSD method. Calculation results are shown in Fig.9 together with results in the HF method where an imaginary part is obtained from a sum of ring diagram calculated by using a nucleon propagator in the HF approximation. A difference between $Im\Sigma_0$ and $Im\Sigma_s$ in the BNSD method is neary equal with one in the HF method as well as the difference $Re\Sigma_0 - Re\Sigma_s$, though the difference is slightly larger in the HF method than in the BNSD method. An absolute value of $Im\Sigma$, however, shows a large difference between the two methods. In Fig.10 we show contributions of each meson in $Im\Sigma$. A contribution of ω-meson is prominently large compared with other contributions and a main part of contribution generates from a term with $ImD_t(R) - ImD_l(R)$ in the integral in $Im\Sigma$ as well as in $Re\Sigma$. This ω-meson dominant result in the neighborhood of the Fermi surface agrees with the discussion[12] stated in the non-relativistic HF approximation. Other contributions gave little decrease(increase) to $Im\Sigma_0$ and little increase(decrease) to $Im\Sigma_s$ for a particle state(a hole state), and as a result reduces the difference between $Im\Sigma_0$ and $Im\Sigma_s$.

Fig.9 , Fig.10

Lastly, we calculate Shcrödinger equivalent potentials from the above obtained nucleon self-energies and compare them with the empirical information on a particle state[18] and a hole state[19] in fig.11. Our results are not a fairly well agreement with the data but are not far from the data both in the real part and in the imaginary part. In particular the real part of potential shows a good result. On the other hand the imaginary part of potential is slightly smaller than the data. The dashed line in the figure shows the contribution of one-bubble (lowest order) diagram. We note that the higher order corrections have a tendency to reduce imaginary potential.

Fig.11

5. Remarks and summary

We can remove the instability in the vicinity of the normal density by introducing the vacuum polarization of σ-meson at low momentum transfer. Though this vacuum polarization shows an important role for removal of liquid-vapor instability, this polarization gives a little contribution to energy density. The vacuum polarization shows a positive and nearly constant value under our approximation and so seems to consistent with the small σ-meson mass without the vacuum polarization of meson. It is still difficult to remove the above instability in the low density and this suggests that a surface of nucleus can not be approximated as a low density limit of nuclear matter.

In the calculation of optical potential the objective nucleon enters into nuclear medium with low incident energy and interacts strongly with nucleons in nuclear matter, and so in this paper we assume that the incident nucleon occupies a particle state formed already in nuclear matter. The higher an incident energy is, the more different the dispersion relation of incident nucleon is with the one of constituent nucleon of nuclear matter.

The ω-meson contribution to the quantum part of nucleon self-energy is prominently large in comparison with other contributions. In $Re\Sigma$ the other contributions cancel out each other, and in $Im\Sigma$ the σ-meson contribution is very small and the contribution of $\sigma-\omega$ mixing reduces the differnce between $Im\Sigma_0$ and $Im\Sigma_s$. This ω-meson dominance is generated from the term having the difference of two components of ω-meson propagator in the integral in nucleon self-energy. We note that the difference of two components vanishes without nuclear medium effect on ω-meson. The ω-meson dominance has the effective mass of nucleon increase rapidly in the incident energy region $|E - M| < -B.E.$(=15.7MeV).

This ω-meson dominance in the nucleon self-energy does not leave marks in the energy density per nucleon.We note that the relative values and signs of differences,$Re\Sigma_0^\sigma$ -$Re\Sigma_s^\sigma$, $Re\Sigma_0^\omega$ -$Re\Sigma_s^\omega$, and $Re\Sigma_0^{\sigma-\omega}$ -$Re\Sigma_s^{\sigma-\omega}$ correspond to $\epsilon_{SD,\sigma}$,$\epsilon_{SD,\omega}$ and $\epsilon_{SD,M}$ respectively.

The imaginary optical potential was reduced by adding ring diagrams in higher order, and is slightly smaller than the recent experimentally extracted data[20]. There are other processes to cause a imaginary potential, and as an example we have a process by which a particle state decays into 3p-2h states. This process is evaluated by introducing the lowest vertex correction in the nuclear Schwinger-Dyson formalism.

The difference of Σ_0 and Σ_s is nearly same in the BNSD method and the HF method, but the sum of them is different between the two methods,i.e., in the energy-dependence near the Fermi surface in the real part and in the absolute value in the imaginary part. A spin-orbit potential is related to the sum of Σ_0 and Σ_s. Then, we want to evaluate the spin-orbit potential in the two methods. However, the spin-orbit potential includes a radial differentiation. Unfortunately, we can not use results of nuclear matter to obtain the spin-orbit potential in the space expression by adopting the local density approximation since the BNSD method dose not assure stability of nuclear matter at low density.

Acknowledgment

The authors are grateful to Prof. Kohmura, Prof. Kumano, N. Noda and N. Kakuta for usuful discussions, and to the menbers of nuclear theorist group in Kyushu district in Japan for their continuous encouragement. The authors also gratefully acknowledge the computing time granted by the Research Center for Nuclear Physics(RCNP).

References

1) C.Bedau and F.Beck, Nucl.Phys.**A560**(1993),518.

2) X.JI, Phys.Lett.**B208**(1988),19.

3) R.Furnstahl, R.J.Perry and B.D.Serot, Phys.Rev.**C40**(1990),321.

4) K.Lim,Ph.D.Thesis in the Dept.of Phys.Indiana Univ.(1990),
K.Lim and C.J.Horowitz, Nucl.Phys.**A501**(1989),729.

5) M.Prakash, P.J.Ellis and J.I.Kapusta, Phys.Rev.**C45**(1992),2518.

6) J.A.MacNeil, C.E.Price and J.R.Shepard, Phys.Rev.**C47**(1993),1534.

7) M.P.Allendes and B.D.Serot, Phys.Rev.**C45**(1992),2975.

8) M.Nakano and A.Hasegawa, Phys.Rev.**C43**(1991),613.

9) M.Nakano, A.Hasegawa, H.Kouno and K.Koide, Phys.Rev.**C49**(1994),3061.

10) M.Nakano, K.Koide, T.Mitsumori, M.Muraki, H.Kouno and A.Hasegawa,
Phys.Rev.**C49**(1994),3067.

11) A.Hasegawa, K.Koide, T.Mitsumori, M.Muraki, H.Kouno and M.Nakano,
Prog.Theor.Phys.Vol.**92**(1994),331.

12) J.P.Blaizot and B.L.Friman, Nucl.Phys.**A372**(1981),69.

13) J.D.Walecka, Ann.of Phys.**83**(1974),491.

14) L.S.Celenza, A.Pantziris and C.M.Shakin, Phys.Rev.**C45**(1992),205.

15) G.Q.Li and R.Machleidt, Phys.Rev.**C48**(1993),1062.

16) C.J.Horowitz, Nucl.Phys.**A412**(1984),228.

17) B.D.Serot and J.D.Walecka, Advance in Nuclear Physics Vol.16,"The
relativistic Nuclear Many-Body Problem"(Plenum Press, New York, 1986).

18) B.Friedmann and V.R.Pandharipande, Phys.Lett.**100B**(1981),205.

19) C.Mahaux and N.Ngo, Phys.Lett.**100B**(1981),285.

20) M.Matoba etal, Pyhs.Rev.**C48**(1993),95.

Table and Figure captions

Table Couplings searched in the BNSD method and in the HF method, and internal terms in energy density per nucleon ($\epsilon = E/\rho_B$, in MeV) at the normal density (k_F=1.42 fm^{-1}).

Fig.1 Diagrammatic representation of nuclear Schwinger-Dyson equations. Double solid (wavy) lines represent exact nucleon(meson) propagators, while single solid(wavy) lines represent free ones. Γ_a denotes a vertex function.

Fig.2 Feynman diagrams taken into account in the calculation of nucleon self-energy, (a) diagrams for real self-energy and (b) diagram for imaginary self-energy. Upward and Downward lines denote particle and hole states respectively.

Fig.3 Meson self-energies as a function of transferd energy q_0 by fixing a transferd momentum q=100 MeV, (a) and (b) for real parts and (c) for imaginary parts. In figs.(a) and (b) solid(dotted) lines denote self-energies including(excluding) meson polarization.

Fig.4 Saturation curve in binding energy.

Fig.5 Dielectric function at zero energy transfer as a function of momentum q. The dotted line denotes the result without the vacuum polarization.

Fig.6 Real part of nucleon self-energies calculated by the BNSD method (solid lines) and by the HF method(dotted lines).

Fig.7 Contributions of σ-meson, ω-meson and $\sigma - \omega$ mixing in real part of nucleon self-energy.

Fig.8 Meson propagators as a function of transfer energy R_0 by fixing a transferd momentum R=100 MeV, (a) for real parts and (b) for imaginary parts.

Fig.9 Imaginary part of nucleon self-energies calculated by the BNSD method(solid lines) and by the HF method(dotted lines).

Fig.10 Contributions of σ-meson, ω-meson and $\sigma - \omega$ mixing in imaginary part of nucleon self-energy.

Fig.11 Energy-dependence of Schrödinger equivalent potential (a) in a real part and (b) in a imaginary part in comparison with the empirical information[18),19)]. In Fig.11(b) the dotted line denotes the result contributed only from the one-bubble diagram.

Table

	g_s	g_v	$\epsilon_B - M$	$\epsilon_{C,\sigma}$	$\epsilon_{C,\omega}$	$\epsilon_{SD,\sigma}$	$\epsilon_{SD,\omega}$	$\epsilon_{SD,M}$	$\epsilon_{SD}/\epsilon_C \times 100$
BNSD	9.120	11.00	-39.2	170.6	-145.9	-10.7	-7.6	17.2	4.7%
HF	9.130	10.412	-40.4	173.1	-131.8	-36.9	20.2	0	40%

Fig.1

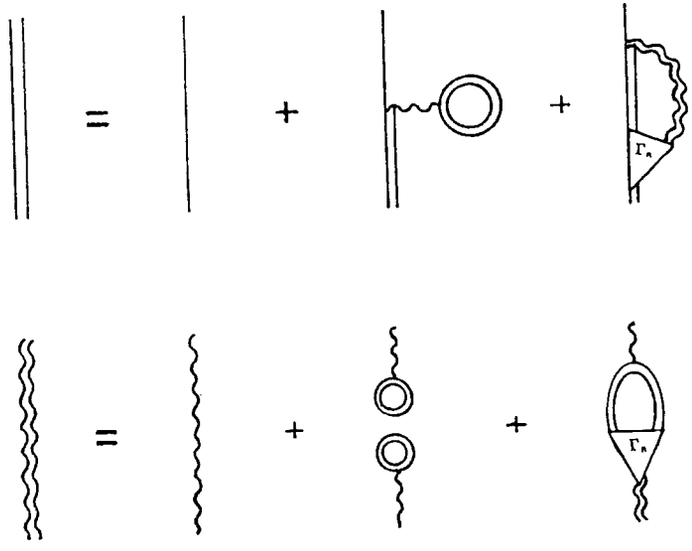

Fig.2

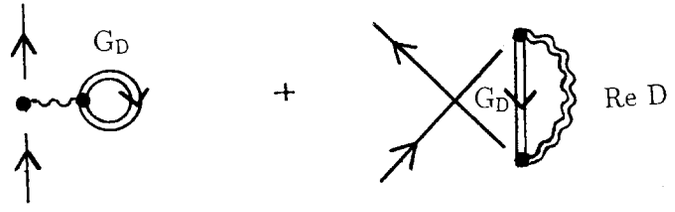

(a)

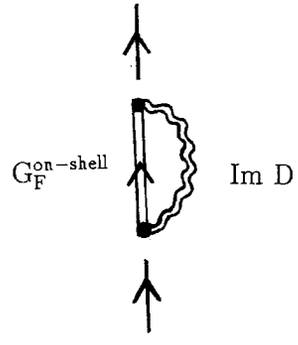

(b)

Fig.3(a)

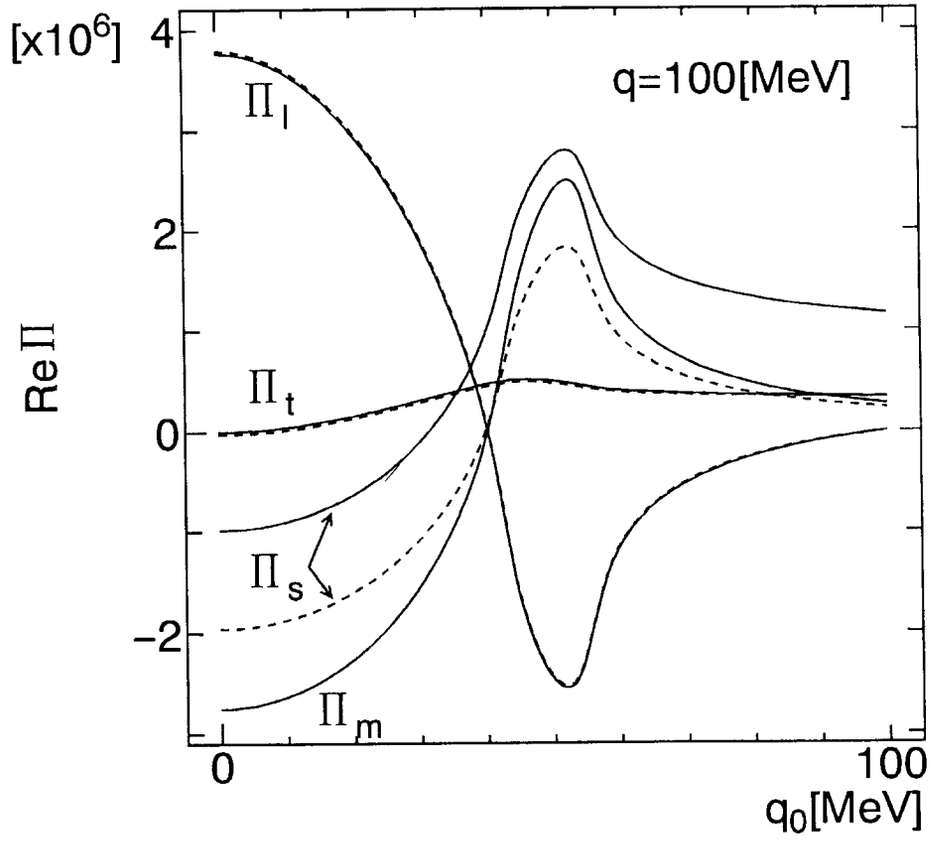
[x10^6]
4
2
0
−2
Re Π
q=100[MeV]
Π_l
Π_t
Π_s
Π_m
0
100
q_0[MeV]

Fig.3(b)

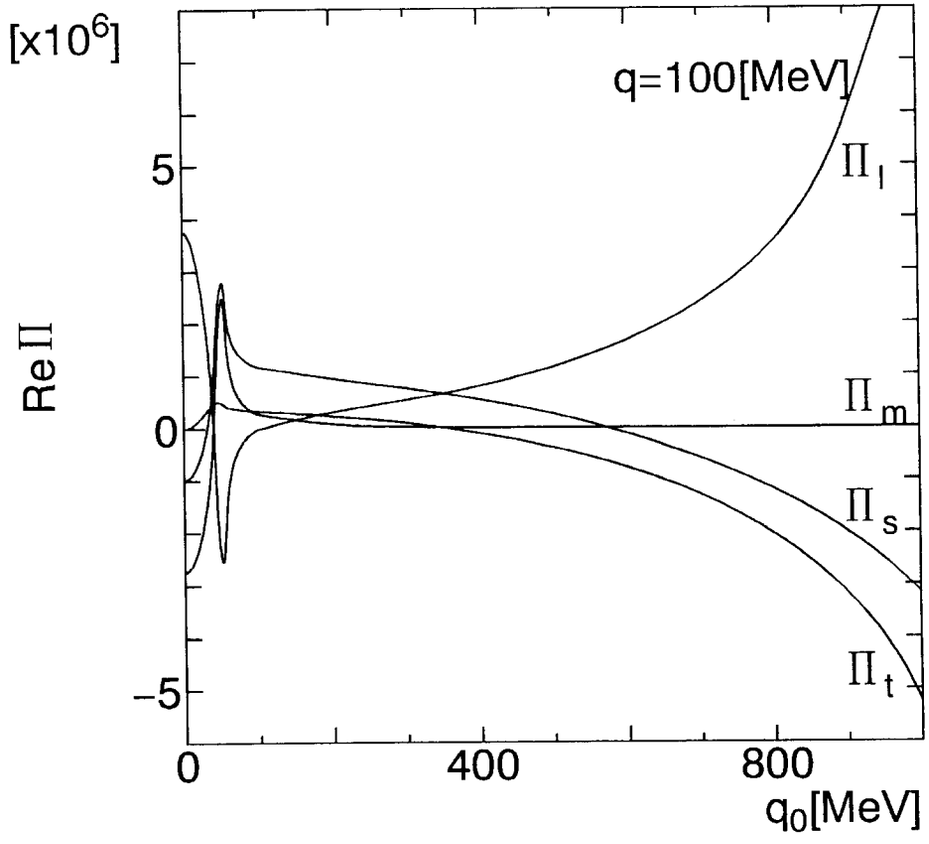
[x10^6]
5
0
−5
Re Π
q=100[MeV]
Π_l
Π_m
Π_s
Π_t
0
400
800
q_0[MeV]

Fig.3(c)

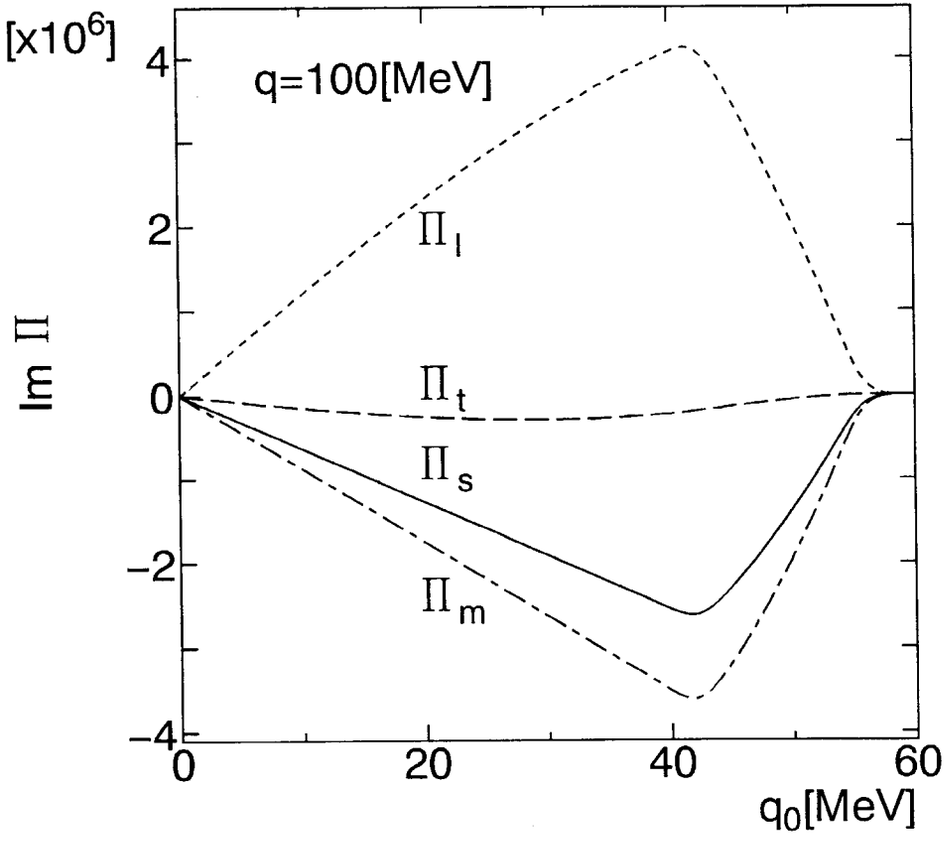
[x10^6]
q=100[MeV]
Im Π
Π_l
Π_t
Π_s
Π_m
4
2
0
−2
−4
0
20
40
60
q_0[MeV]

Fig.4

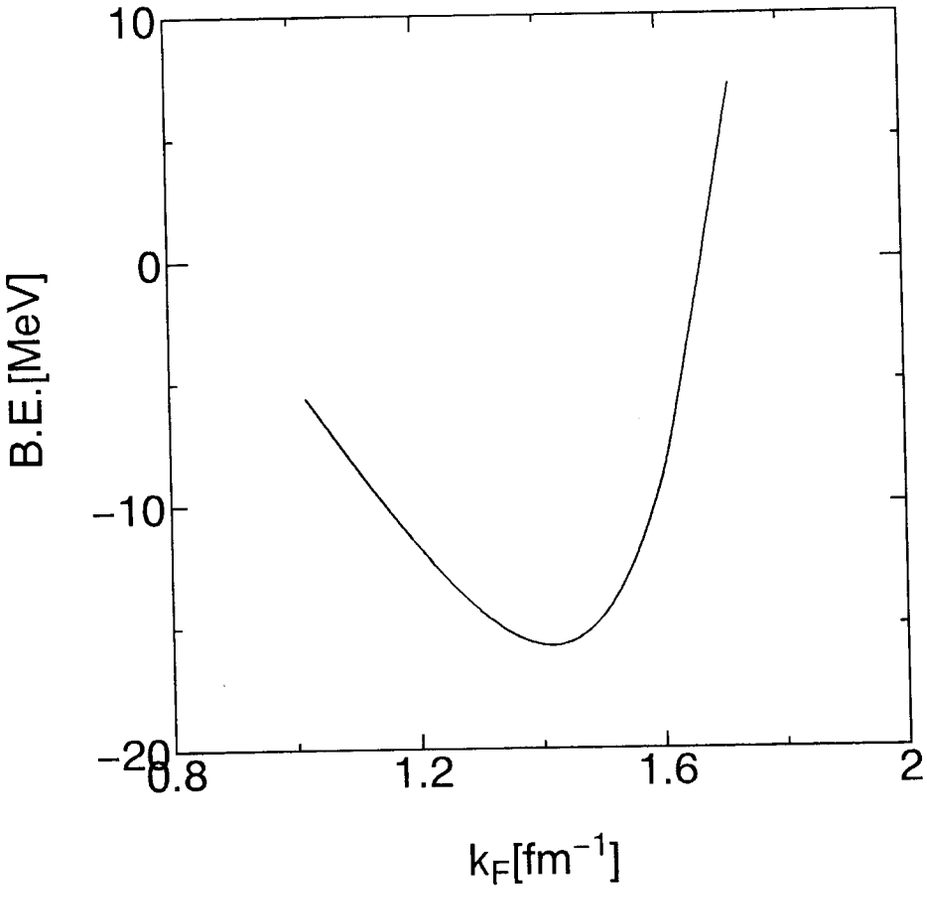
B.E.[MeV]
10
0
−10
−20
0.8
1.2
1.6
2
k_F[fm^−1]

Fig.5

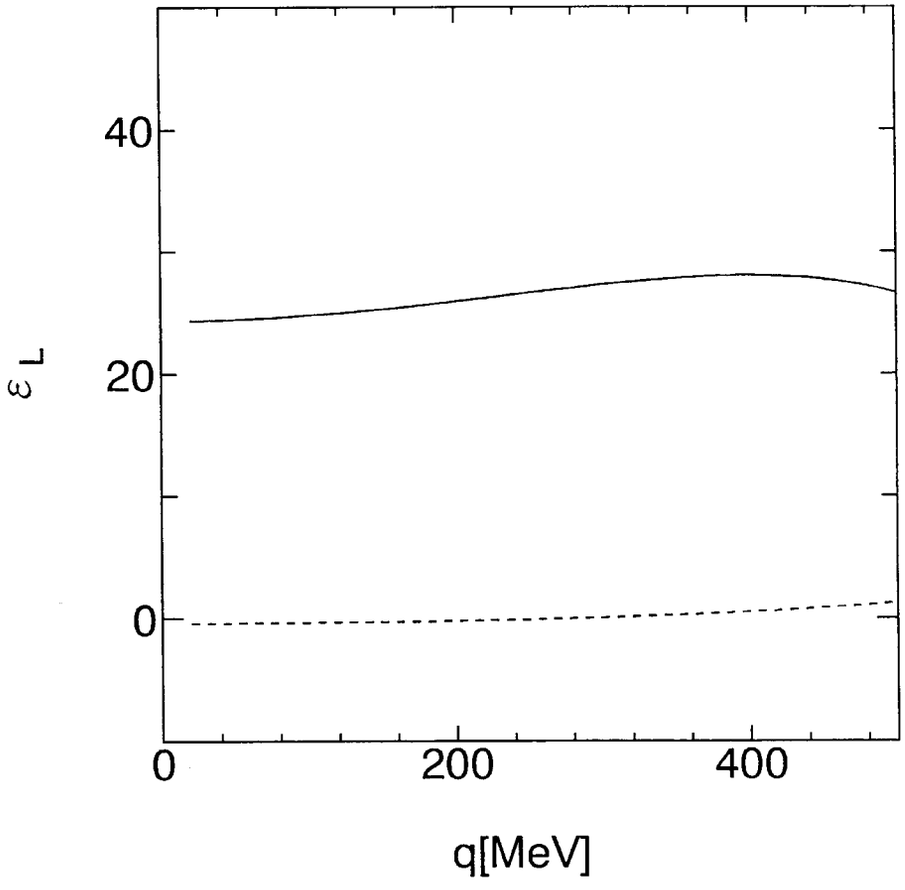
40
20
0
ε_L
0
200
400
q[MeV]

Fig.6

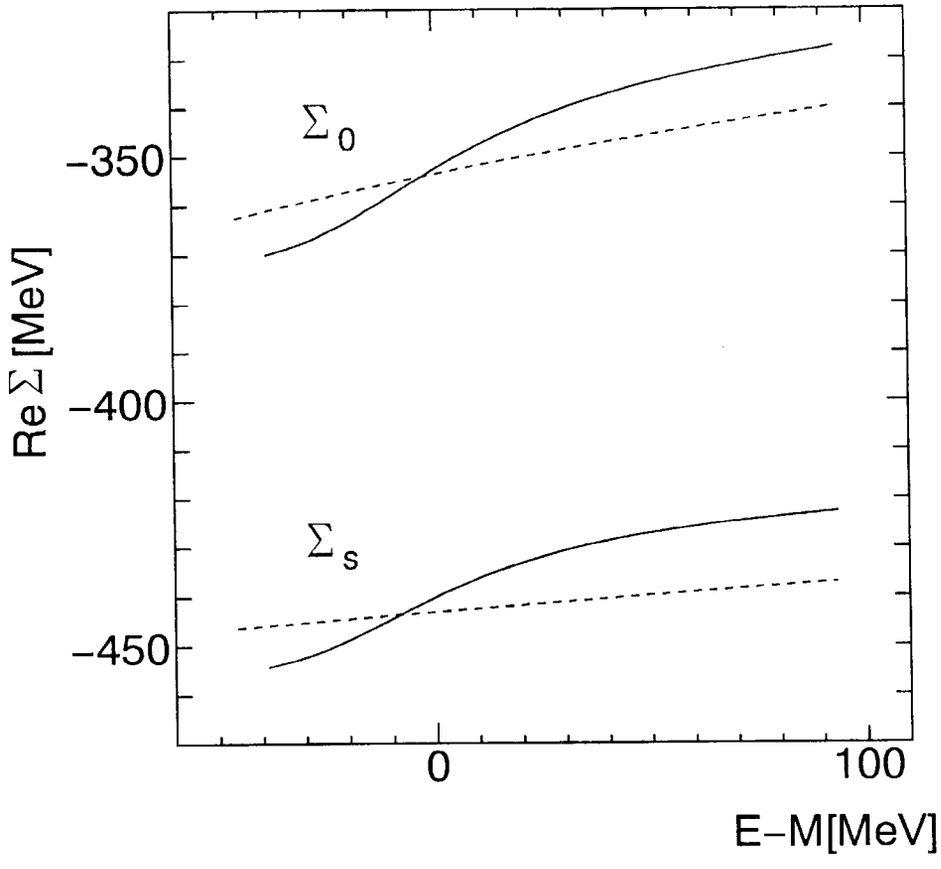
Σ_0
Σ_s
−350
−400
−450
Re Σ [MeV]
0
100
E−M[MeV]

Fig.7

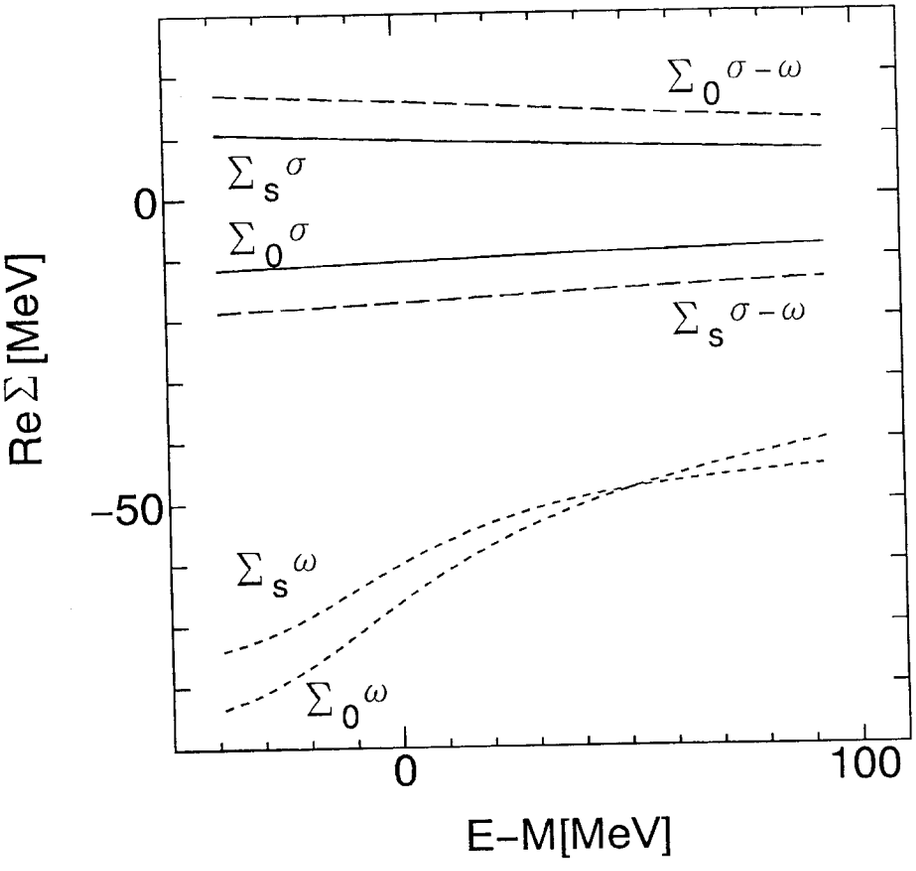
Re Σ [MeV]
0
−50
0
100
E−M[MeV]
Σ0σ−ω
Σsσ
Σ0σ
Σsσ−ω
Σsω
Σ0ω

Fig.8(a)

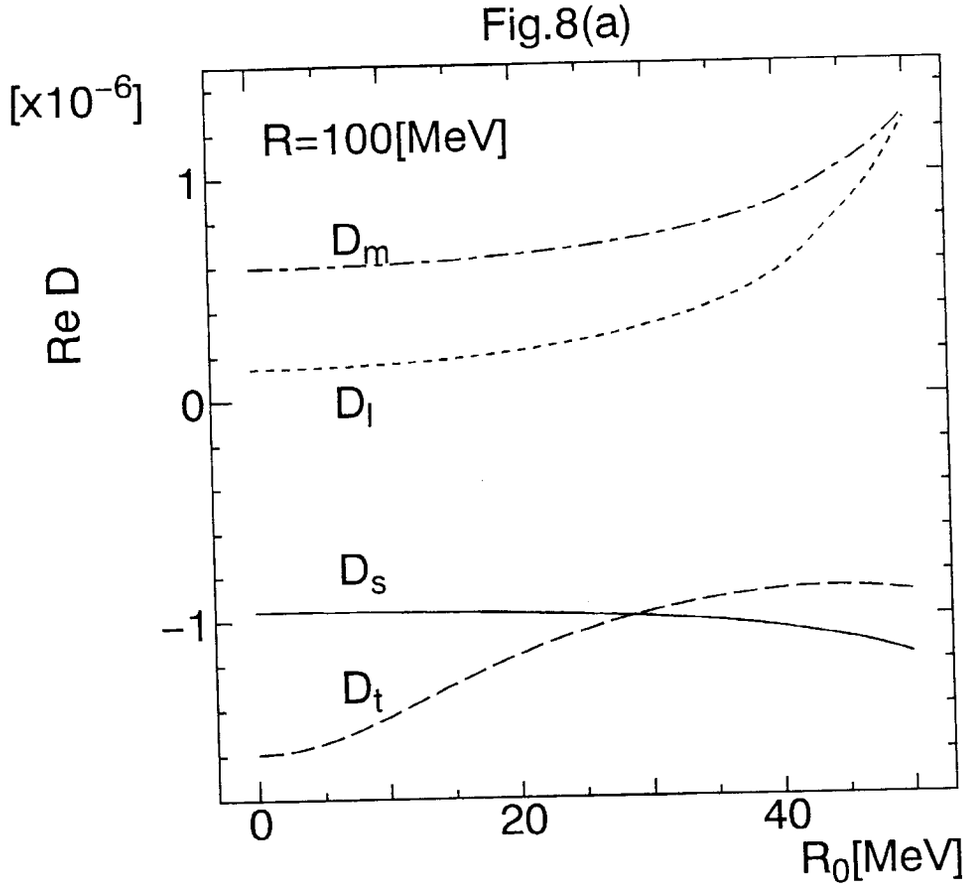
[x10−6]
Re D
R=100[MeV]
1
0
−1
Dm
Dl
Ds
Dt
0
20
40
R0[MeV]

Fig.8(b)

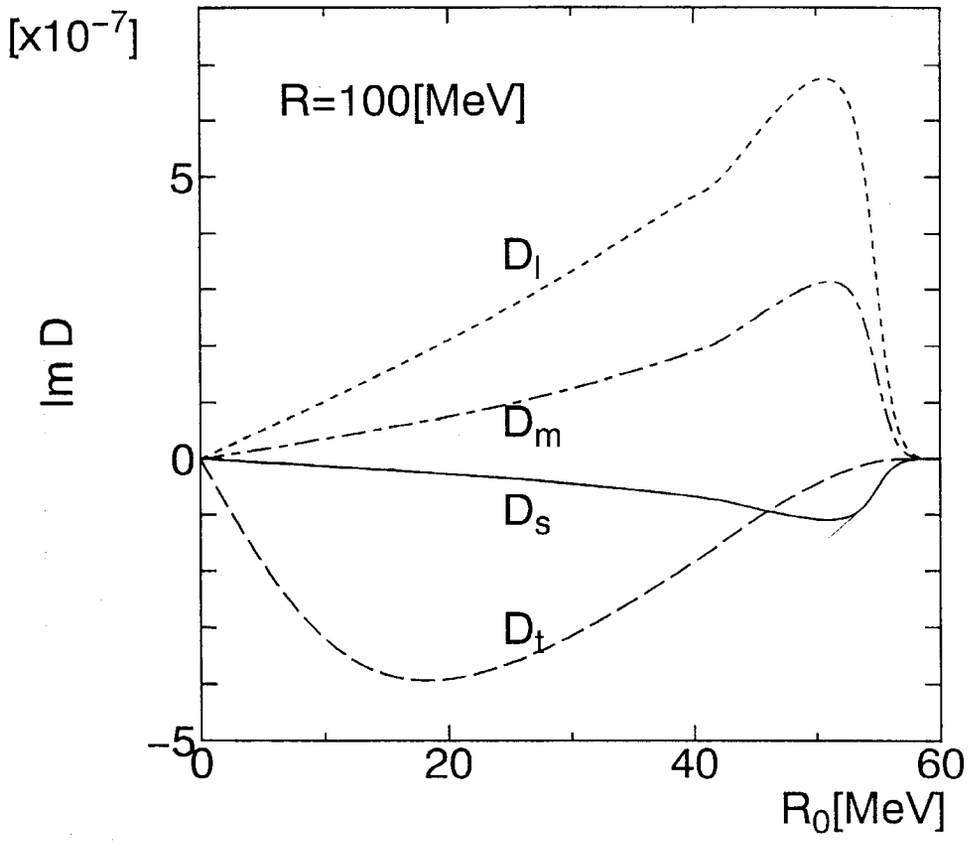
[x10^{-7}]
R=100[MeV]
5
0
−5
Im D
D_l
D_m
D_s
D_t
0
20
40
60
R_0[MeV]

Fig.9

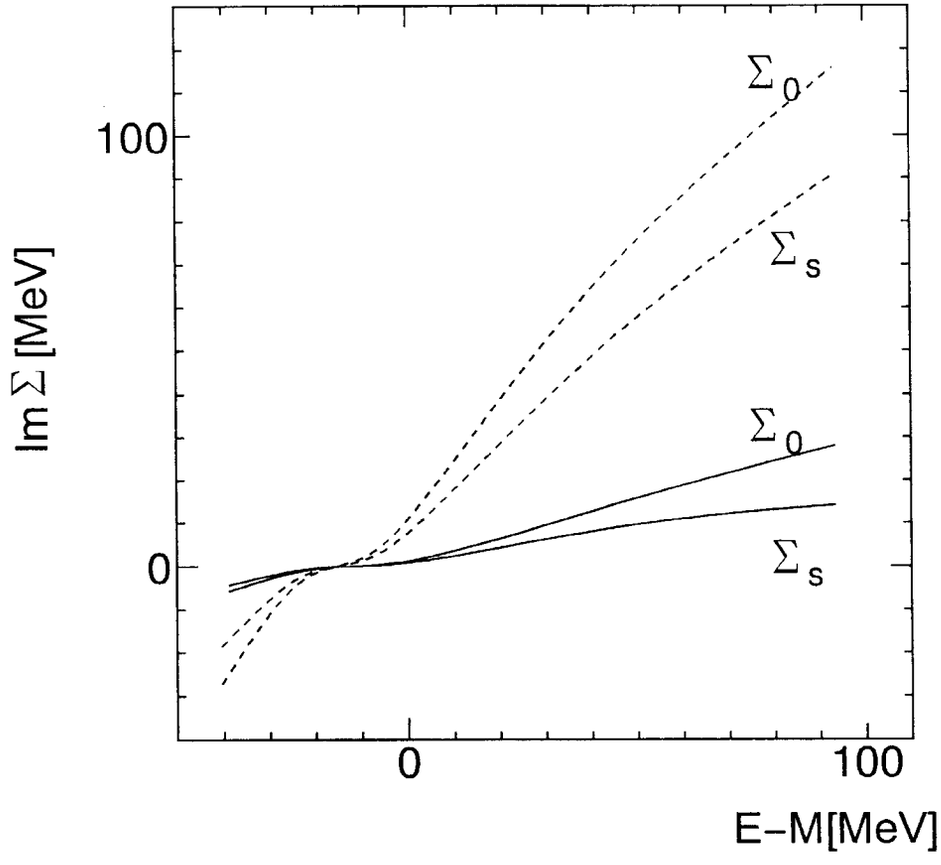
100
0
Im Σ [MeV]
Σ_0
Σ_s
Σ_0
Σ_s
0
100
E−M[MeV]

Fig.10

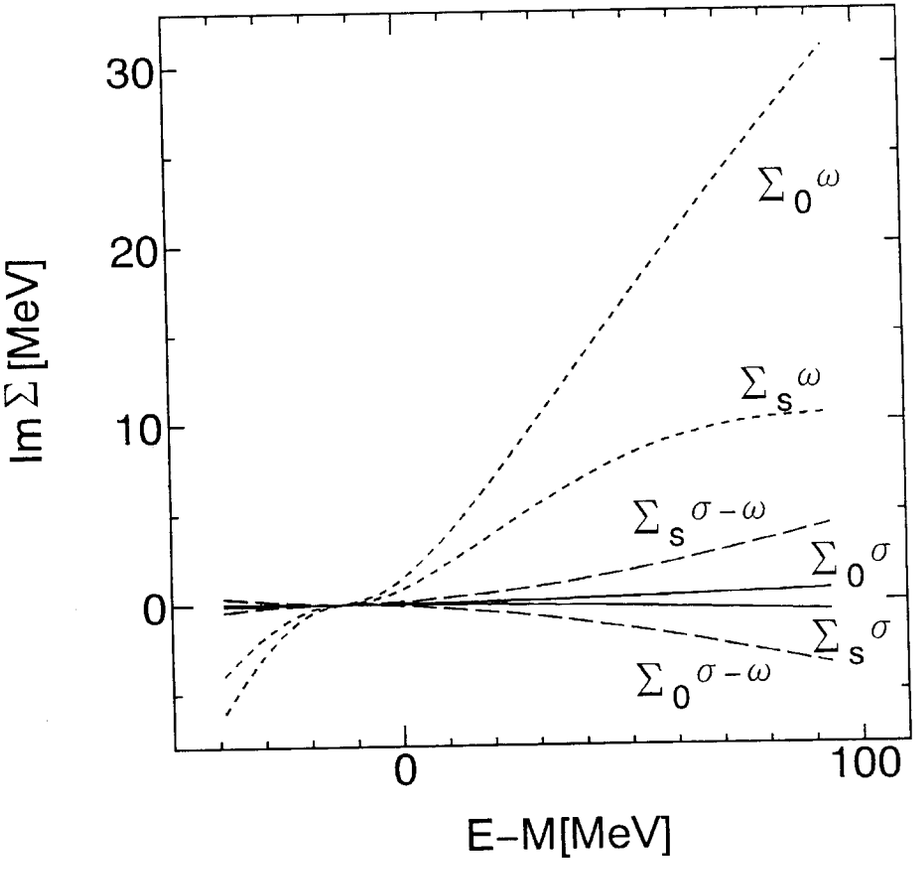

Fig.11(a)

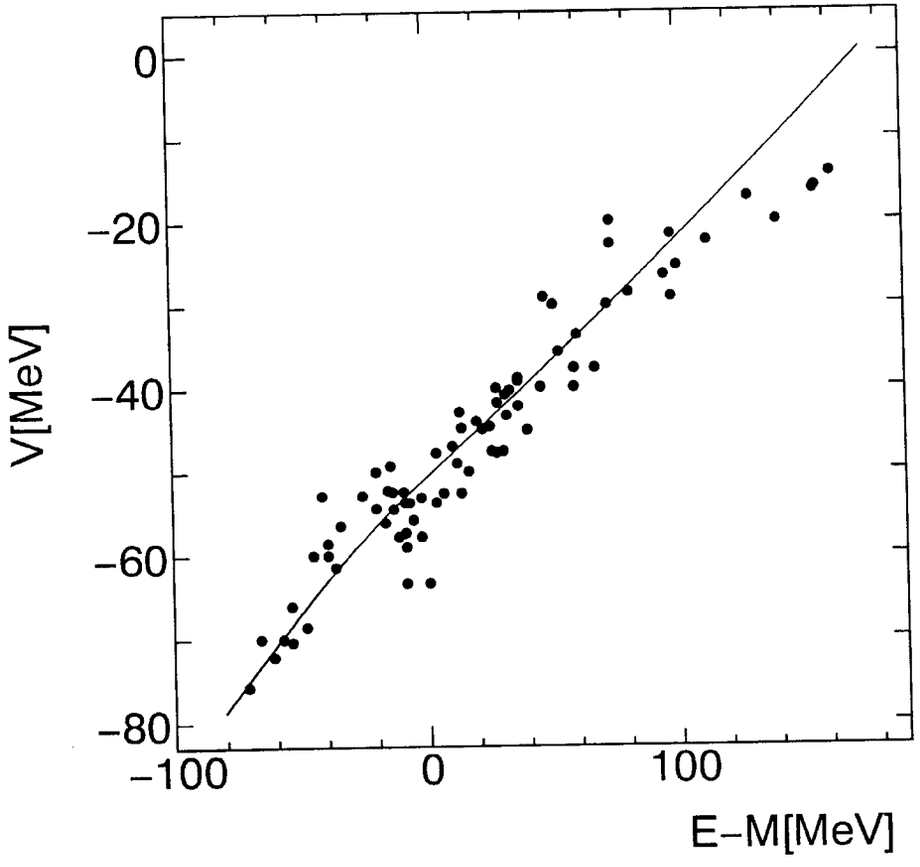

Fig.11(b)